Contents

1

Pattern Formation in Nonequilibrium Systems

1.1 Introduction

In contrast to equlibirum systems systems far from equilibrium can exhibit the spontaneous formation of spatial, temporal, and spatio-temporal structures. These structures emerge by processes of spontaneous self-organization without being imposed from the outside. A paradigam of such systems is *Rayleigh-Bénard convection*. It consists of a fluid layer heated from below under the influence of gravity. If the temperature difference between lower and upper fluid boundary is small, heat is transported by heat conduction. If the temperature difference exceeds a certain threshold macroscopic fluid motion sets in. This motion may have different structures, depending on the fluid properties, the applied temperature difference, and the nature of the vertical and horizontal fluid boundaries. For an extensive discussion we refer the reader to the review article of E. Bodenschatz, W. Pesch, and G. Ahlers in Annual Reviews of Fluid Mechanics **32**, 709 (2000).

Similar patterns can be observed in the light field produced by suitably designed lasers. As is well-known, the transition towards Laser action is due to self-organization, (c.f. H. Haken, *Synergetics. An Introduction*). In recent years, pattern formation in the transverse field of lasers has been under intensive experimental investigations, see the review article by T. Arecchi (F.T. Arecchi, S. Bocalletti, P.L. Ramazza, Physics Reports 318, 1 (1999)).

Other examples of patterns are observed in reaction diffusion systems, where they are denoted as Turing structures as well as in gas-discharge systems (H. G. Purwins, Sh. Amiranashvili, Selbstorganisierte Strukturen im Strom, Phys. J. 6, 21 (2007)).

In the following we shall summarize some interesting spatio-temporal patterns which can be observed in Rayleigh-Bénard system. Then we shall discuss a class of equations, the so-called Swift-Hohenberg equations, which are used for the investigation of pattern formation in quasi two dimensional systems, i.e. systems like Rayleigh-Bénard convection in systems whose horizontal ex-

tensions are large in comparision to the cell thickness (so-called large aspect ratio systems).

The Swift-Hohenberg equations can be numerically treated by pseudo-spectral methods. These numerical calculations can be used to get acquainted with pattern formation in nonequilibrium systems, pattern selection, and the emergence of complex spatio-temporal patterns.

References:

E. Bodenschatz, W. Pesch, and G. Ahlers, Recent Development in Rayleigh-Bénard Convection, Annual Reviews of Fluid Mechanics **32**, 709 (2000)
H. Haken, *Synergetics. An Introduction.* (Springer-Verlag)
F.T. Arecchi, S. Bocalletti, P.L. Ramazza, Physics Reports 318, 1 (1999
H. G. Purwins, Sh. Amiranashvili, Selbstorganisierte Strukturen im Strom, Phys. J. 6, 21 (2007)

1.2 Patterns in Rayleigh-B'enard Convection

Figures (1.1), (1.2), (1.3) exhibit spatial structures which can be observed in careful experiments on Rayleigh-Bénard convection. They emerge from initial conditions as stationary patterns in time and are characterized by well-ordered spatial structures, which reminds one on two dimensional crystal structures. However, in contrast to crystals, they only are formed under nonequilibrium conditions. The questions which immediately arise concern the question of the selection of the wavelength of the patterns and the planform, i.e. the question, what type of crystal structures emerge. Furthermore, fig. (1.4) demonstrates the existence of patterns with nontrivial topology generated by defects in the roll structures.

The fact that pattern formation in Rayleigh-Bénard convection is a far from equilibrium phenomena becomes evident by the observation of patterns, which undergo permanent temporal evolution without the tendency to approach a final, stationary pattern. Corresponding temporal patterns can become rather complicated. An example of the so-called spiral turbulence state is depicted in figure (**??**). It is a challenge to understand the physical processes leading to permanently evolving structures.

The mentioned phenomena are only few examples from the world of nonequilibrium pattern formation. It seems that there exist universal phenomena, i.e. spatio-temporal patterns which arise in quite different systems. This points to the fact that such types of phenomena can be described by the same mathematical structures which are independent on the specific porperties of the considered systems. The corresponding mathematical evolution equations are the Swift-Hohenberg equations, the Newell-Whitehead-Segel equations and the real and complex Ginzburg-Landau equations.

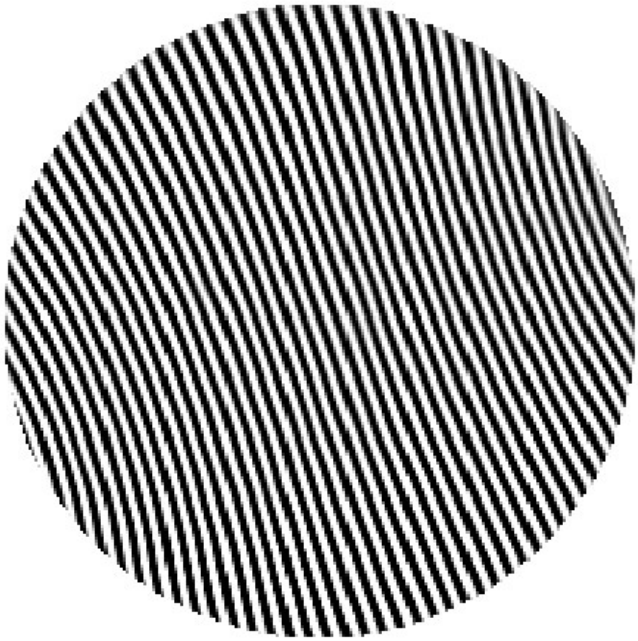

Fig. 1.1. Convection patterns: Rolls.

The pictures of the experimental convection patterns are taken from the Homepage of E. Bodenschatz, as well as the review article of Bodenschatz et al.

1.3 The Order Parameter Concept

Self-organization in systems far from equilibrium can be approached by the order parameter concept, which is a generalization of the Ginzburg- Landau theory of phase transitions in equilibrium systems. It can be summarized as follows.

We consider a pattern forming system described by a state vector $\mathbf{q}(t)$, which consists e.g. of the velocity field, the temperature field and the pressure in the case of Rayleigh Bénard system. It obeys an evolution equation in forms of partial differential equation

$$\dot{\mathbf{q}}(\mathbf{r}, t) = \mathbf{N}[\nabla, \mathbf{q}(\mathbf{r}, t)] \tag{1.1}$$

These are, e.g. the basic fluid dynamical equations.

The long term behaviour of the state vector $\mathbf{q}(\mathbf{r}, t)$ of a system undergoing a process of pattern formation can be represented as a functional of a so-called order parameter, denoted by $\psi(t)$

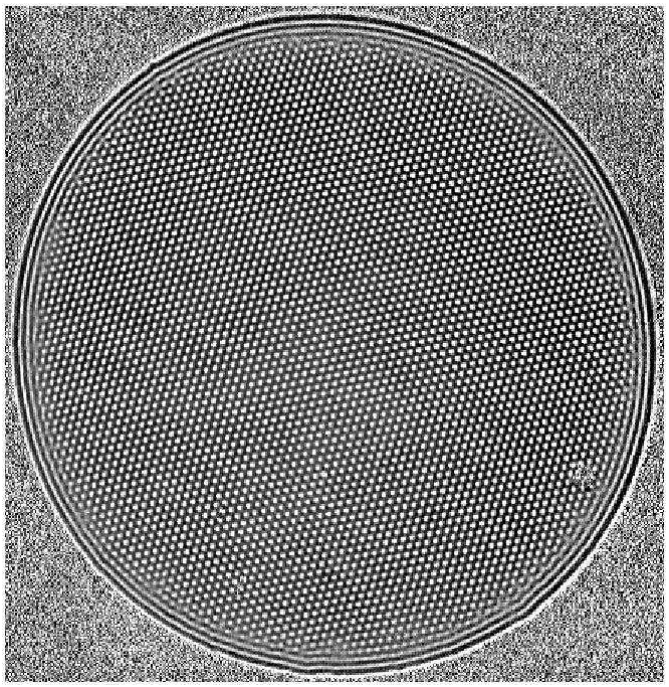

Fig. 1.2. Convection patterns: Hexagons

$$\mathbf{q}(\mathbf{r}, t) = \mathbf{Q}[\psi(t)] \tag{1.2}$$

Instead of solving the determining equations for the state vector $\mathbf{q}(\mathbf{r}, t)$ the spatio-temporal behaviour is determined by an evolution equation for the order parameter $\psi(t)$

$$\dot{\psi} = h[\psi(t)] \tag{1.3}$$

Quite often, the order parameter can be directly related to a physical observable. In the case of the Rayleigh-Bénard experiment we can identify the order parameter $\psi(\mathbf{x}, t)$ as the temperature field in a horizontal plane in the convection box. For laser systems exhibiting pattern formation in the transverse light field the order parameter is related to the electric field amplitude. The validity of the order parameter concept can be proofed for systems close to instabilities, where the system's behaviour changes qualitatively. In these situations the order parameter can be identified and the corresponding order parameter dynamics can be derived from the basic evolution equations. On the other hand, the order parameter dynamics quite often can be established relying on phenomenological arguments combined with symmetry considerations. We refer the reader to the monograph of H. Haken.

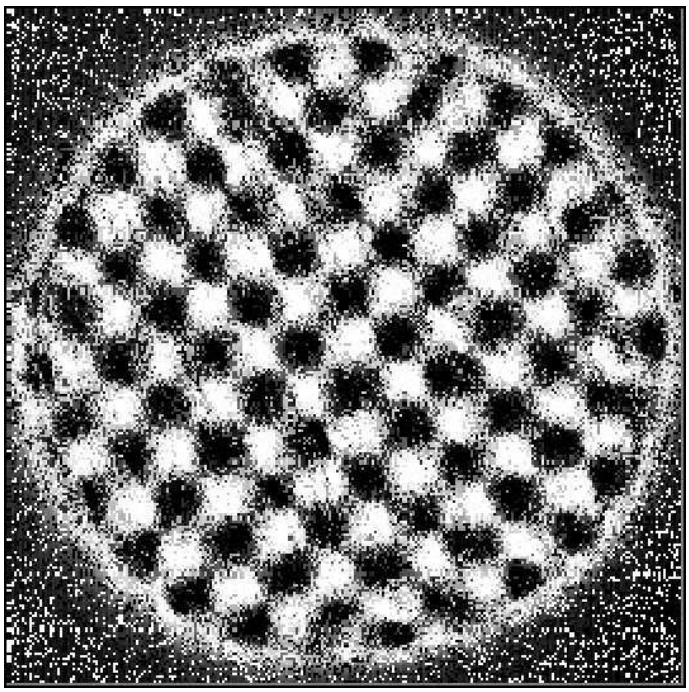

Fig. 1.3. Convection patterns: Squares

1.4 Swift-Hohenberg Equation

The Swift-Hohenberg equation describes the spatio-temporal evolution of a real order parameter field $\psi(\mathbf{x}, t)$ and takes the form

$$\dot{\psi}(\mathbf{x}, t) = \left[\epsilon - \left(k_c^2 + \Delta\right)^2\right] \psi(\mathbf{x}, t) + \delta\psi(\mathbf{x}, t)^2 - \psi(\mathbf{x}, t)^3 \tag{1.4}$$

Additionally, one has to formulate suitable boundary conditions. Usually, one assumes the existence of periodic boundary conditions

$$\begin{aligned} \psi(x, y, t) &= \psi(x + L, y, t) \\ \psi(x, y, t) &= \psi(x, y + L, t) \end{aligned} \tag{1.5}$$

However, as we shall see, boundaries have a strong influence on the global organization of the patterns.

Furthermore, it is important to notice that the Swift-Hohenberg equation (1.38) is invariant with respect to rotations of the coordinate system, as well as reflections.

From a qualitative point of view the Swift-Hohenberg equation as an order parameter equation can be motivated on the basis of the following facts.

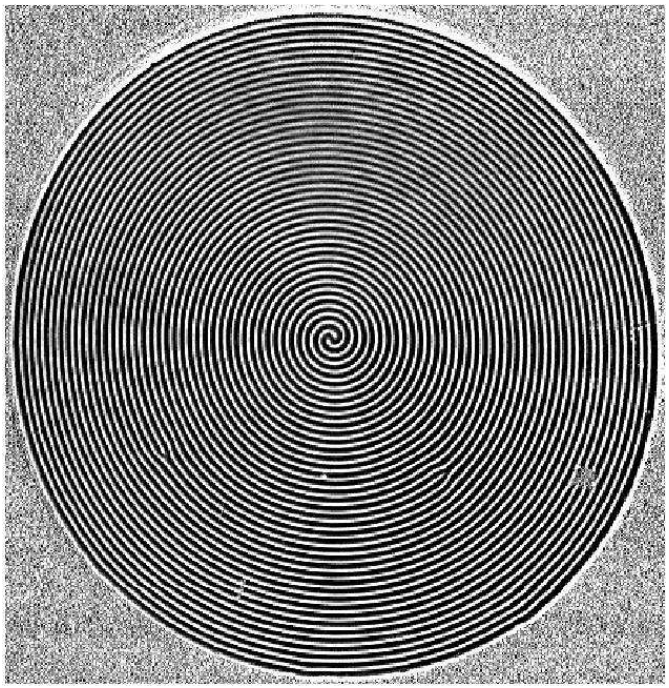

Fig. 1.4. Convection patterns: Giant spiral patterns

1. Instability and Linear Growth of Modes

The patterns show the occurrence of a certain wavelenght. Decomposing the order parameter field into plane waves

$$\psi(\mathbf{x},t) = \sum_{\mathbf{k}} \xi_{\mathbf{k}}(t) \frac{1}{\sqrt{V}} e^{i\mathbf{k}\cdot\mathbf{x}} \tag{1.6}$$

This can be modeled by a linear growth of amplitudes $\xi_{\mathbf{k}}(t)$ with wave vector with lenght close to wave number k_c:

$$\xi_{\mathbf{k}}(t) = e^{\lambda(\mathbf{k})t} \tag{1.7}$$

The growth rates should be positive for amplitudes with $|\mathbf{k}| \approx k_c$, whereas for other amplitudes it should be negative. This property can be achieved, for instance, by taking

$$\lambda(\mathbf{k}) = \epsilon - \left[k_c^2 - \mathbf{k}^2\right]^2 \tag{1.8}$$

The growth rate depends on the wave vector $\mathbf{k}$. Due to rotational symmetry it is a function of $k = ||\mathbf{k}||$. It is depicted in figure (**??**) for the cases $\epsilon < 0$ and $\epsilon > 0$. For $\epsilon < 0$ the growth rate for values of k are negative and the order parameter $\psi(\mathbf{x},t)$ tends to zero under the evolution of the linear equation

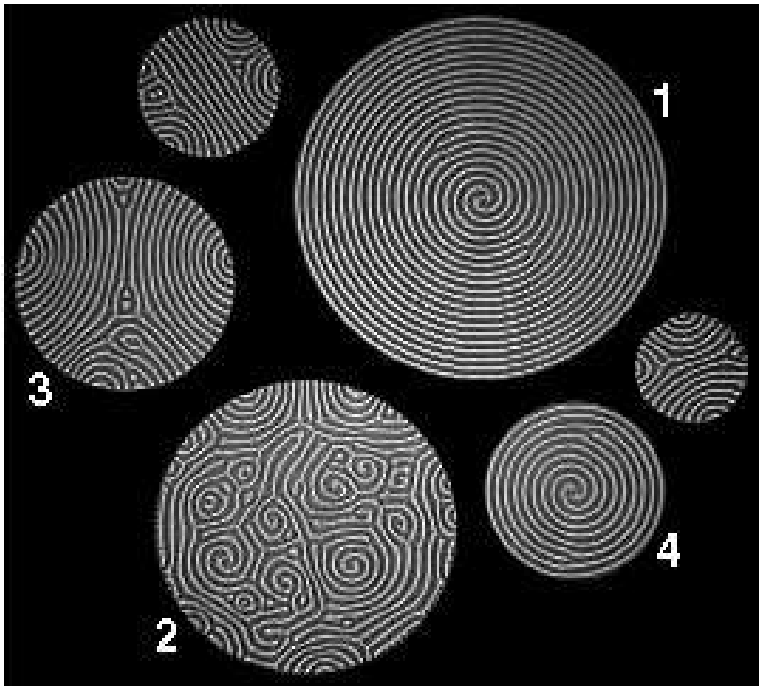

Fig. 1.5. Convection patterns: From Single Spirals to Spiral Turbulence

(1.7). For $\epsilon > 0$ disturbances with wave vectors $\mathbf{k}$ with absolute value $k \approx k_c$ get positive growth rate $\lambda(k)$ indicating that the corresponding modes grow exponentially in time.

We consider a two dimensional domain. Then all modes with $\mathbf{k}$-vectors with absolute value taken from a ring of width $\sqrt{\epsilon}$ close to k_c are unstable. The solution of the linear equation would be a superposition of all these modes given by the initial condition

$$\psi(\mathbf{x}, t) = \sum_{\mathbf{k}} \psi(\mathbf{k}, 0) \frac{1}{\sqrt{V}} e^{i\mathbf{k}\cdot\mathbf{x}} e^{\lambda(k)t} \tag{1.9}$$

In real space, the evolution equation reads

$$\dot{\psi}(\mathbf{x}, t) = \left[\epsilon - \left[k_c^2 + \Delta\right]^2\right] \psi(\mathbf{x}, t) \tag{1.10}$$

2. Nonlinear Saturation and Selection of Patterns

The exponential growth or deacy of the mode amplitudes (1.10) has to be modified leading to a *saturation* of the amplitudes. This can be achieved by adding suitable nonlinearities to the linear equation. A simple choice is to take

$$N = \delta\psi(\mathbf{x}, t) - \psi(\mathbf{x}, t)^3 \tag{1.11}$$

However, it turns out, that the choice of the nonlinear functional $N[\psi]$ not only leads to a saturation of the linear growth but also is responsible for the *selection of patterns*, i.e. the formation of stripes, hexagons, squares or more complicated patterns.

We can also perform the discussion in $\mathbf{k}$-space. The linear growth of modes (1.7) is modified leading to a saturation of the amplitudes. In a naive way, one can extend the differential equation of the amplitudes by the inclusion of a nonlinear term

$$\dot{\xi}_{\mathbf{k}}(t) = \left[\epsilon - \left[k_c^2 - \mathbf{k}^2\right]^2\right] \xi_{\mathbf{k}}(t) - |\xi_{\mathbf{k}}(t)|^2 \xi_{\mathbf{k}}(t) \tag{1.12}$$

This would lead to the saturation of the amplitudes with positive growth rates in the long term limit

$$|\xi_{\mathbf{k}}(t)|^2 = \left[\epsilon - \left[k_c^2 - \mathbf{k}^2\right]^2\right] \tag{1.13}$$

whereas modes with negative growth rate die out. However, in order to allow for mode interactions, one should include in general the cubic terms

$$\dot{\xi}_{\mathbf{k}}(t) = \lambda(\mathbf{k}\xi_{\mathbf{k}}(t) - \sum_{\mathbf{k}_1,\mathbf{k}_2,\mathbf{k}_3} \Gamma_{\mathbf{k};\mathbf{k}_1,\mathbf{k}_2,\mathbf{k}_3} \xi_{\mathbf{k}_1}(t)\xi_{\mathbf{k}_2}(t)\xi_{\mathbf{k}_3}(t) \tag{1.14}$$

where the mode coupling coefficients $\Gamma_{\mathbf{k};\mathbf{k}_1,\mathbf{k}_2,\mathbf{k}_3}$ have to be choosen appropriately.

The mode coupling coefficient for the nonlinearity $\psi^3(\mathbf{x},t)$ is given by

$$\begin{aligned} \Gamma_{\mathbf{k};\mathbf{k}_1,\mathbf{k}_2,\mathbf{k}_3} &= \int d\mathbf{x} \frac{e^{i[-\mathbf{k}+\mathbf{k}_1+\mathbf{k}_2+\mathbf{k}_3]\mathbf{x}}}{V^2} \xi_{\mathbf{k}_1}(t)\xi_{\mathbf{k}_2}(t)\xi_{\mathbf{k}_3}(t) \\ &= \frac{1}{V}\delta_{\mathbf{k},\mathbf{k}_1+\mathbf{k}_2+\mathbf{k}_3} \xi_{\mathbf{k}_1}(t)\xi_{\mathbf{k}_2}(t)\xi_{\mathbf{k}_3}(t) \end{aligned} \tag{1.15}$$

As we shall see the special form of the nonlinearity decides about the selection of the patterns.

Square patterns are obtained from the nonlinearity

$$N[\psi] = \nabla \cdot \left[\psi \left(\nabla\psi\right)^2\right] \tag{1.16}$$

The corresponding equation is denoted as Gertsberg- Shivashinsky equation and can be derived for large aspect ratio Rayleigh Bénard systems in the presence of poorly heat conductive states.

In the following we shall consider order parameter equations of the form

$$\dot{\psi}(\mathbf{x},t) = \left[\epsilon - \left(k_c^2 + \Delta\right)^2\right] \psi(\mathbf{x},t) + N\left[\psi\right] \tag{1.17}$$

Here $N\left[\psi\right]$ denotes a nonlinear functional of the order parameter field $\psi(\mathbf{x},t)$. A discussion of the order parameter equations can be found in:

M. Bestehorn, R. Friedrich Rotationally invariant order parameter equations for natural patterns in nonequilibrium systems, Phys. Rev. E 59, 2642 (1999)

1.5 Variational Versus Nonvariational Equations

The Swift-Hohenberg equation (1.38) can be expressed in variational form

$$\dot{\psi}(\mathbf{x},t) = -\frac{\delta}{\delta\psi(\mathbf{x},t)} V\left[\psi(\mathbf{x},t)\right] \tag{1.18}$$

with the Ljapunov functional

$$V = \int d\mathbf{x}\{\frac{1}{2}\left[(k_c^2+\Delta)\psi(\mathbf{x},t)\right]^2 - \frac{\epsilon}{2}\psi(\mathbf{x},t)^2 + \frac{1}{4}\psi(\mathbf{x},t)^4\} - \frac{\delta}{3}\psi(\mathbf{x},t)^3 \tag{1.19}$$

This is an important property since the stable stationary states are determined by the local minima of this functional. The existence of a Ljapunov functional yields properties which are well-known from systems in thermal equilibrium. States of equilibrium systems are extremal states of a thermodynamic potential, e.g. the free energy. Similarly, patterns of a nonequilibrium systems having a Ljapunov functional are determined by the minima of this functional. However, we shall point out that this functional may have a great variety of different minima. This makes the study of such systems highly interesting. Furthermore, we may consider order parameter equations, which can not be expressed in variational form. As we shall see this will lead to spatio-temporal chaos.

1.6 Numerical Treatment: Pseudo-Spectral Methods

Numerically, the Swift-Hohenberg equation can be solved in a straight forward manner by pseudo-spectral method.

1.6.1 Periodic Boundaries

For the numerical treatment of the order parameter equation (1.17) one could convert it into a set of amplitude equations of the form (1.14). However, the evaluation of the sum over the mode coupling coefficients would be extremely time consuming. In this case, the use of a pseudo-spectral methods is straight forward.

Fourier transform of the Swift-Hohenberg equation leads to

$$\dot{\psi}(\mathbf{k},t) = L(-k^2)\psi(\mathbf{k},t) + N(\mathbf{k},t) \tag{1.20}$$

where $N(\mathbf{k},t)$ denotes the Fourier transform of the nonlinearity. For the standard nonlinearity we explicitly obtain

$$N(\mathbf{k},t) = \frac{1}{\sqrt{V}} \int d\mathbf{x} e^{-i\mathbf{k}\cdot\mathbf{x}} \left[\delta\psi(\mathbf{x},t)^2 - \psi(\mathbf{x},t)^3\right] \tag{1.21}$$

1.6.2 Inclusion of Boundaries

The pseudo-spectral method is designed for the treatment of patterns for domains in the presence of periodic boundary conditions. However, a variety of pattern forming properties depend on the geometry of the considered domain and the corresponding boundary conditions.

An elegant method to introduce boundaries consist of the inclusion of so-called ramps. The idea of a ramp is also utilized in experiments. In Rayleigh-Bénard convection this would simply correspond to a nonuniform heating of the layer from below in such a way that the system becomes subcritical outside a certain domain. Numerically, this can can be achieved by introducing a space-dependent control parameter

$$\epsilon = \epsilon_0 + \epsilon_1(\mathbf{x}) \tag{1.22}$$

The contribution $\epsilon_1(\mathbf{x})$ is negative outside the domain under consideration leading to a damping of the patterns in the outer region. The computation can then be performed using periodic boundary conditions.

We emphasize that, especially in convection experiments, the proper treatment of boundaries is a rather delicate subject. The introduction of a ramp is a special case of so-called penalty methods.

1.7 Examples: Stripes

Figure (1.6) exhibits the temporal evolution of the solution of Swift-Hohenberg equation ($\delta = 0$) starting from random initial conditions

$$\psi(\mathbf{x}, t) = \psi(\mathbf{x}, 0) \tag{1.23}$$

where $\psi(\mathbf{x}, 0)$ is a random number from taken from the interval $-\sqrt{\epsilon} \leq \psi(\mathbf{x}, 0) \leq \sqrt{\epsilon}$. One observes the selection of *stripes*. However, the evolving pattern contains dislocations and grain boundaries between regions with differently oriented stripes.

1.7.1 Amplitude Equation for Stripes

We try to calculate the solution of the stripe patterns analytically. To this end we consider $\delta = 0$ and perform the ansatz

$$\psi(\mathbf{x}, t) = A(t)e^{ik_0 x} + c.c. \tag{1.24}$$

In this representation, the amplitude A is a function of time. Inserting this ansatz into the Swift-Hohenberg equation one obtains

$$[\dot{A} - \epsilon A + 3A|A|^2]e^{ik_0 x} = -A^3 e^{3ik_0 x} - 3A^*|A|^2 e^{-3ik_0 x} + c.c. \tag{1.25}$$

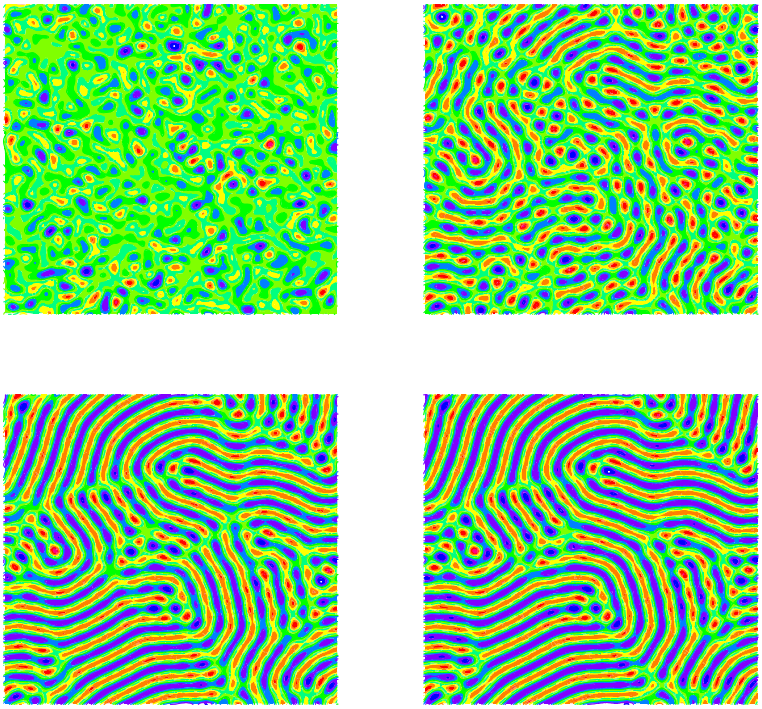

Fig. 1.6. Numerical Calculation of the evolution of stripe patterns from the Swift-Hohenberg equation (1.38) ($\delta = 0$, $\epsilon = .3$)

We see that our ansatz produces terms proportional to e^{3ik_0x} indicating that the ansatz (1.26) is not sufficient and should be extended to include higher terms

$$\psi(\mathbf{x}, t) = A(t)e^{ik_0x} + A_3(t)e^{i3k_0x} + A_5(t)e^{i5k_0x}... + c.c. \tag{1.26}$$

However, if one assumes that the higher order amplitudes are smaller than the leading amplitude A one can determine A from the amplitude equation

$$\dot{A} = (\epsilon - (k_c^2 - k_0^2)^2)A - 3A|A|^3 \tag{1.27}$$

There are stripe solutions

$$A = \sqrt{\frac{\epsilon - (k_c^2 - k_0^2)^2}{3}} \tag{1.28}$$

provided the growth rate $\epsilon - (k_c^2 - k_0^2)^2$ is positive.

However, as we shall discuss in the next subsection, the stripes are not stable for an arbitray wave number k_0.

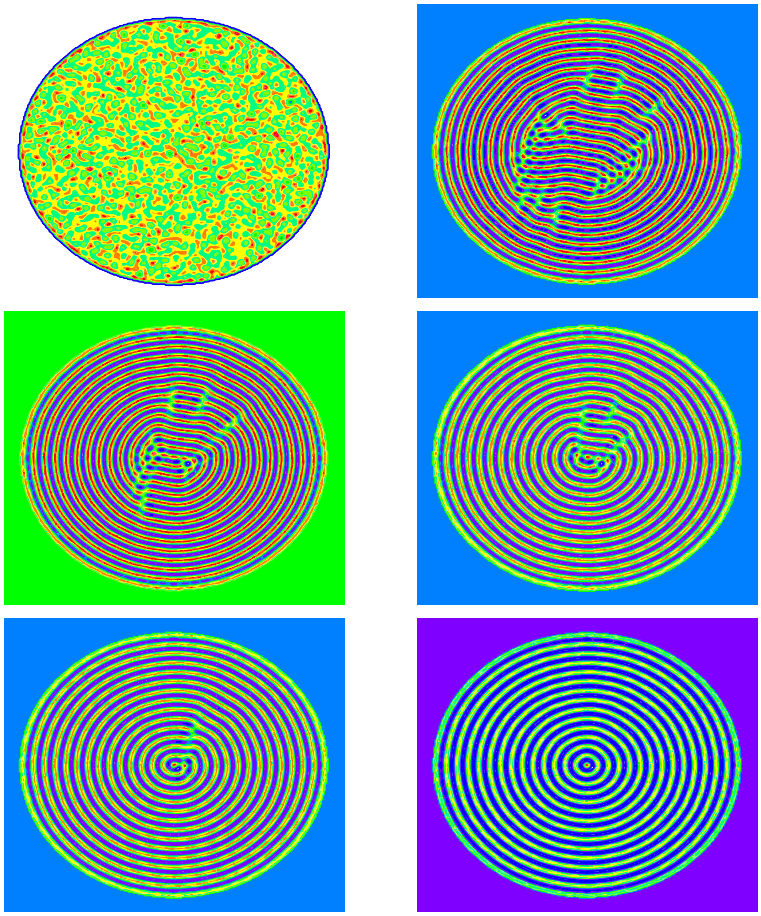

Fig. 1.7. Numerical Calculation of the evolution of stripe patterns from the Swift-Hohenberg equation (1.38) ($\delta = 0$, $\epsilon = .3$). Patterns evolve in a circular domain using a ramp.

1.7.2 Envelope Equation

Now, we extend our treatment to the case, where the amplitude is a slowly varying function of $\mathbf{x}$. Since we can include deviations from the wave number in the amplitude $A(\mathbf{x}, t)$, we can choose $k_0 = k_c$:

$$\psi(\mathbf{x}, t) = A(\mathbf{x}, t)e^{ik_c x} + c.c. + O(A^3) \tag{1.29}$$

We have to include the spatial variations in the form

$$\frac{\partial}{\partial x} A(\mathbf{x}, t)e^{ik_c x} = e^{ik_c x} \left(\frac{\partial}{\partial x} + ik_c \right) A(\mathbf{x}, t)$$

$$\frac{\partial}{\partial y}A(\mathbf{x},t)e^{ik_c x} = e^{ik_c x}\frac{\partial}{\partial y}A(\mathbf{x},t) \tag{1.30}$$

This leads us to the expansion

$$\left(k_c^2 + \Delta\right) = \left(2ik_c\frac{\partial}{\partial x} + \frac{\partial^2}{\partial x^2} + \frac{\partial^2}{\partial y^2}\right)^2 \approx \left(2ik_c\frac{\partial}{\partial x} + \frac{\partial^2}{\partial y^2}\right)^2 \tag{1.31}$$

Here, we have taken into account that for slight spatial distortions of the stripe solution the second derivative in x-direction is small compared to the other terms.

Finally we end up with the so-called Newell-Whitehead-Segel equation

$$\dot{A} = \left[\epsilon + 4k_c^2(\frac{\partial}{\partial x} - \frac{i}{2k_c}\frac{\partial^2}{\partial y^2})^2\right] A - 3A|A|^2 \tag{1.32}$$

Based on this equation, we can now calculate so-called *long wave instabilities* of the stripe patterns. To this end we consider stripe solutions characterized by the wave number $\tilde{k} = k_c + k$

$$A = A_k e^{ikx} \tag{1.33}$$

and investigate small deviations

$$\begin{aligned} A &= A_k e^{ikx} + a_\kappa e^{ikx+i\kappa x} e^{\lambda t} \\ A^* &= A_k^* e^{-ikx} + b_\kappa e^{-ikx+i\kappa x} e^{\lambda t} \end{aligned} \tag{1.34}$$

We obtain the linear set of equations

$$\begin{aligned} \lambda a &= [\epsilon - (2k_c(k+\kappa) + \kappa_y^2)^2 - 2A_k^2]a - A_k^2 b \\ \lambda b &= [\epsilon - (2k_c(-k+\kappa) + \kappa_y^2)^2 - 2A_k^2]b - A_k^2 a \end{aligned} \tag{1.35}$$

The characteristic equation reads

$$\Lambda^2 + \Lambda[(k_c^2 - (k+\kappa)^2)^2 + (k_c^2 - (k-\kappa)^2)^2] - A_k^4 = 0 \tag{1.36}$$

The eigenvalues are explicitly given by

$$\lambda_{1,2} = \epsilon - 2A_k^2 + ... \tag{1.37}$$

From this expression we can read off the existence of the following two instabilities.

Zig-Zag Instability

As can be seen, straight rolls with $k < 0$, i.e. rolls with wavelength larger than the critical one, are unstable with respect to perturbations in transversal direction. This is the so-called Zig-Zag instability. The temporal development of a a stripe pattern, which is zigzag unstable, is exhibited in fig: (1.8). Loosely speaking the stripes, which are too wide with respect to the critical wavelength try to decrease their wavelenght by forming zig-zag like patterns. The resulting patterns contain grain boundaries as well as defects, and exhibit a temporal evolution on a rather slow time sca le

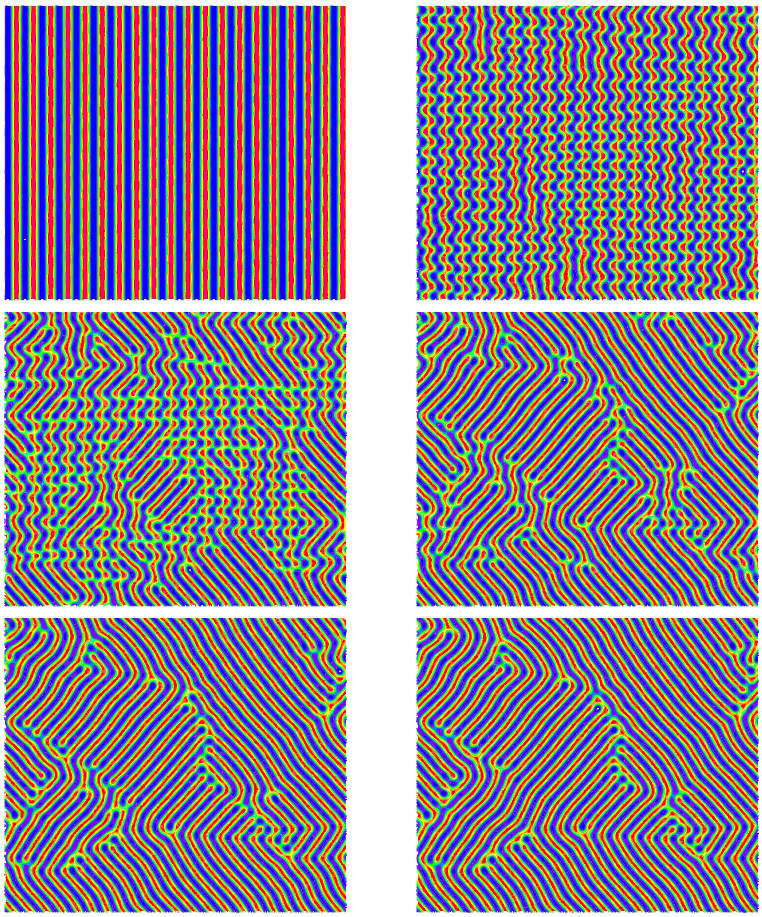

Fig. 1.8. Numerical Calculation of the evolution of stripe patterns from the Swift-Hohenberg equation (1.38) ($\delta = 0$, $\epsilon = .3$). Patterns evolve in a circular domain using a ramp.

Eckhaus Instability

The next instability is the so-called Eckhaus instability. Stripes with wave lenght smaller than the critical one are unstable. Fig. (**??**) demonstrates the spatio-temporal evolution of an Eckhaus-unstable pattern. First, the amplitude of the pattern decreases so that defects can be generated. These defects eventually merge with the consequence that the wavelength of the stripes, which initially was in the Eckhaus unstable regime, returns to the Eckhaus-stable regime.

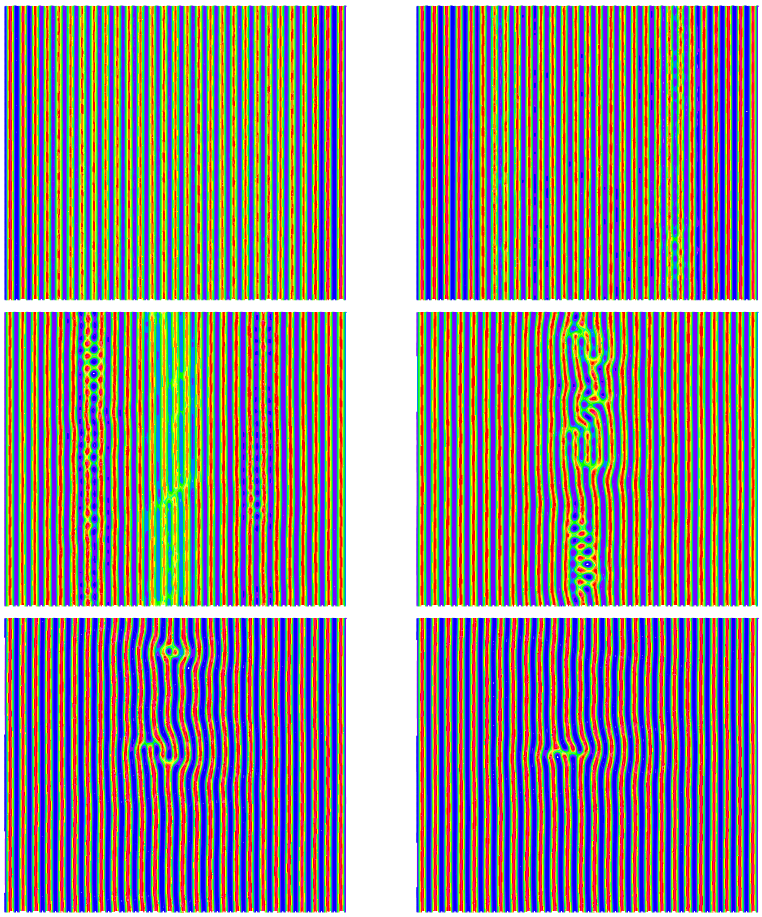

Fig. 1.9. Numerical Calculation of the evolution of stripe patterns from the Swift-Hohenberg equation (1.38) ($\delta = 0$, $\epsilon = .3$). Patterns evolve in a circular domain using a ramp.

1.8 Hexagons

The Swift-Hohenberg equation can be generalized by the inclusion of a quadratic nonlinearity (M. Bestehorn, H. Haken, Phys. Lett. 99A, 265 (1983), Z. Phys. B 57, 329 (1984)). This has the consequence that hexagonal patterns become stable patterns in some parameter regions.

$$\dot{\psi}(\mathbf{x},t) = \left[\epsilon - \left(k_c^2 - \Delta\right)\right]\psi(\mathbf{x},t) + \delta\psi(\mathbf{x},t)^2 - \psi(\mathbf{x},t)^3 \qquad (1.38)$$

The numerical treatment of this equation demonstrates that it is possible to obtain hexagonal patterns in certain regions of the parameter space $[\epsilon, \delta]$. An example is depicted in fig. (1.10). Starting from random initial conditions

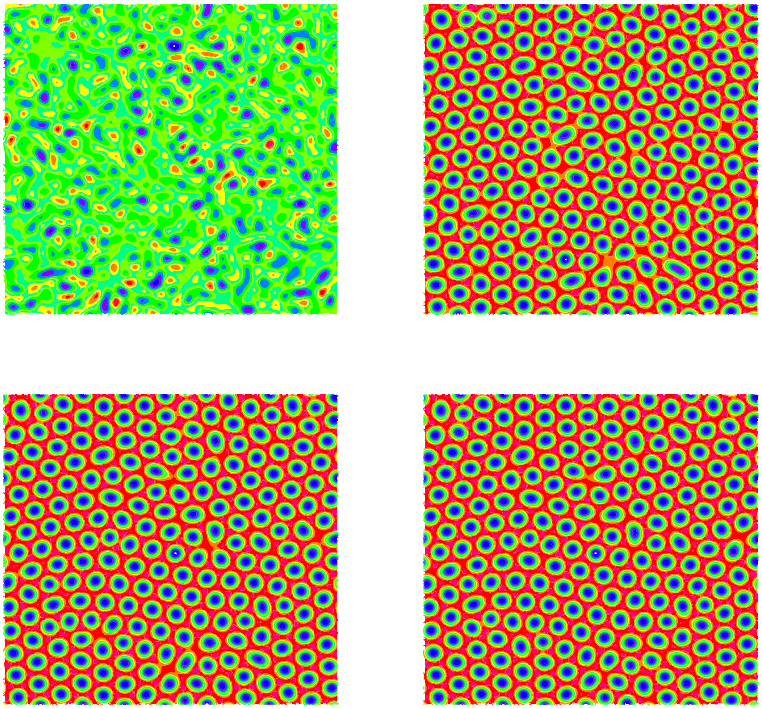

Fig. 1.10. Numerical calculation of the evolution of hexagonal patterns from the Swift-Hohenberg equation (1.38) ($\delta = .1$, $\epsilon = .3$).

we observe the formation of a hexagonal pattern. However, this pattern is not perfectly ordered. It contains defects, so-called penta-hepta defects consisting of a cell surrounded by seven respectively five neigbouring cells.

1.8.1 Stripes Versus Hexagons

The selection of hexagons versus stripes can be investigated on the basis of amplitude equations. In order to derive amplitude equations for the description of hexagons we perform the ansatz

$$\psi(\mathbf{x}, t) = \xi_1 e^{i\mathbf{k}_1 \cdot \mathbf{x}} + \xi_2 e^{i\mathbf{k}_2 \cdot \mathbf{x}} + \xi_3 e^{i\mathbf{k}_3 \cdot \mathbf{x}} + c.c. \tag{1.39}$$

with the three wave vectors

$$\begin{aligned} \mathbf{k}_1 &= k_c(1, 0) \\ \mathbf{k}_2 &= k_c\left(-\frac{1}{2}, \frac{\sqrt{3}}{2}\right) \\ \mathbf{k}_3 &= k_c\left(-\sqrt{\frac{1}{2}}, -\frac{\sqrt{3}}{2}\right) \end{aligned} \tag{1.40}$$

Explicit calculation shows that

$$\psi(\mathbf{x},t)^2 = \xi_1^*\xi_2^* e^{-i(\mathbf{k}_1+\mathbf{k}_2)\mathbf{x}} + \xi_2^*\xi_3^* e^{-i(\mathbf{k}_1+\mathbf{k}_2)\mathbf{x}} + \xi_3^*\xi_1^* e^{-i(\mathbf{k}_1+\mathbf{k}_2)\mathbf{x}} + ... \quad (1.41)$$

Similar expressions arise for the cubic terms.

The resulting amplitude equations are obtained in a similar way as demonstrated for the stripe solutions:

$$\begin{aligned}
\dot{\xi}_1 &= \epsilon\xi_1 + \delta\xi_2^*\xi_3^* - \xi_1\left[a|\xi_1|^2 + b|\xi_2|^2 + b|\xi_3|^2\right] \\
\dot{\xi}_2 &= \epsilon\xi_2 + \delta\xi_3^*\xi_1^* - \xi_2\left[a|\xi_2|^2 + b|\xi_3|^2 + b|\xi_1|^2\right] \\
\dot{\xi}_3 &= \epsilon\xi_3 + \delta\xi_1^*\xi_2^* - \xi_2\left[a|\xi_3|^2 + b|\xi_1|^2 + b|\xi_2|^2\right]
\end{aligned} \quad (1.42)$$

The amplitude equations possess several types of solutions describing different types of patterns. The first type of solutions are the *stripes*. They are obtained from the ansatz

$$\xi_1 = \xi \qquad , \qquad \xi_2 = 0 \qquad , \qquad \xi_3 = 0 \quad (1.43)$$

where the amplitude ξ obeys the amplitude equation

$$\dot{\xi} = \epsilon\xi - a\xi|\xi|^2 \quad (1.44)$$

The solutions are

$$\xi = \sqrt{\frac{\epsilon}{a}} e^{i\Phi} \quad (1.45)$$

The phase Φ remains undetermined, which is due to the fact that the stripe pattern can be translated in space due to translational symmetry. The order parameter field $\psi(\mathbf{x},t)$ takes the form

$$\psi(\mathbf{x},t) = \sqrt{\frac{\epsilon}{a}} cos\left(\mathbf{k}_1 \cdot \mathbf{x} + \Phi\right) \quad (1.46)$$

and we explicitly see that change of the phase Φ corresponds to a shift of the pattern.

We consider now the stability analysis of the stripe solutions. To this end we introduce

$$\xi_1 = \xi + \eta_1 \qquad , \qquad \xi_2 = \eta_2 \qquad , \qquad \xi_3 = \eta_3 \quad (1.47)$$

and obtain the linear set of equations

$$\begin{aligned}
\dot{\eta}_1 &= -\epsilon\eta_1 - \epsilon\eta_1^* \\
\dot{\eta}_2 &= \epsilon(1 - \frac{b}{a})\eta_2 - \delta\eta_3^* \\
\dot{\eta}_3 &= \epsilon(1 - \frac{b}{a})\eta_3 - \delta\eta_2^*
\end{aligned} \quad (1.48)$$

The characteristic equation determining the eigenvalue λ read

$$\lambda_{\pm} = \epsilon(1 - \frac{b}{a}) \pm \delta \tag{1.49}$$

The stripes are linearly stable for values of ϵ larger than

$$\epsilon \leq \frac{\delta}{1 - \frac{b}{a}} \tag{1.50}$$

Hexagon solutions are obtained by the ansatz

$$\xi_1 = \xi_2 = \xi_3 = A^{i\Phi} \tag{1.51}$$

which leads to the single amplitude equation

$$\dot{A} = \epsilon A - \delta A^2 - A^3(a + 2b) \tag{1.52}$$

Nontrivial solutions are

$$A = -\frac{\delta}{2(a+2b)} \pm \sqrt{\frac{\delta^2}{4(a+2b)^2} + \epsilon} \tag{1.53}$$

Stability analysis yield

$$\dot{\eta}_1 = ... \tag{1.54}$$

There are further stationary solutions, the so-called *mixed mode solutions*.

We can summarize our discussions in figure (**??**), which exhibits the bifurcation diagram.

We mention that including slow spatial variations of the amplitudes $\xi_i(\mathbf{x}, t)$ according to the Newell-Whitehead-Segel theory allows one to determine the stability regions of stripes and hexagons with respect to long-wave instabilities as well as to investigate the detailed spatial structure of penta-hepta defects.

1.9 Nonvariational Effects and Pattern Formation

Up to now we have considered evolution equations for which a Ljapunov functional can be formulated. In this section, we consider extensions of the evolution equations, which do not have this important property. As a consequence, it can not expected in generality that the systems tend to stationary patterns with some optimal properties defined by the functional.

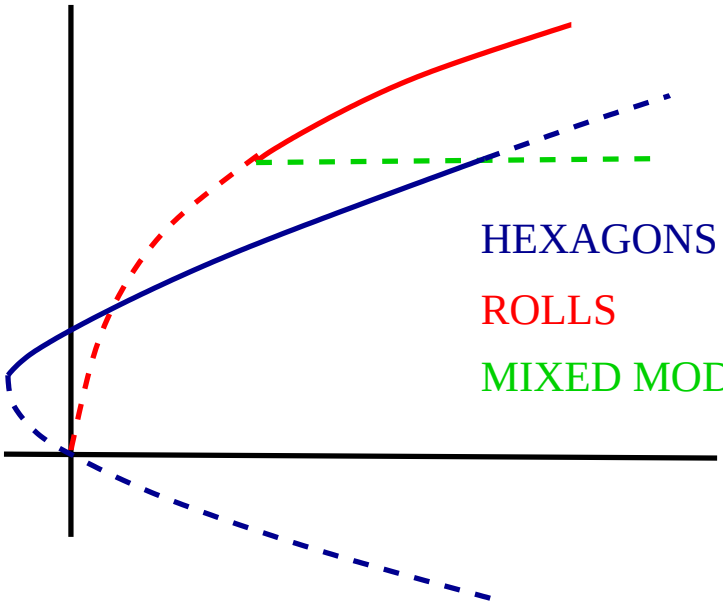

Fig. 1.11. Bifurcation diagram for stripes, hexagons

1.9.1 Model for Rotating Convection

A physically relevant system for a nonvariational system is convection in systems rotating about a vertical axis. Rotation breaks reflection symmetry. Due to the Coriolis force stripe patterns become unstable. This so-called Küppers-Lortz instability leads to spatially and temporally disordered patterns.

(G. Küppers, D. Lortz, Transition from laminar convection to thermal turbulence in a rotating fluid layer, J. Fluid Mech. 35, 609 (1969))

It has been shown that the following model equation for an order parameter field $\psi(\mathbf{x},t)$ is related to convection in rotating large aspect ratio systems (M. Neufeld, R. Friedrich,H. Haken, Order parameter equation and model equation for high Prandtl number Rayleigh-Bénard convection in a rotating large aspect ratio system, Z. Phys. B 92, 243 (1993); M. Neufeld, R. Friedrich, Statistical properties of the heat transport in rotating Bénard convection, Phys. Rev E 51. 2033 (1995); J. Millan-Rodriquez, M. Bestehorn, C. Perez-Garcia, R. Friedrich, M. Neufeld, Defect motion in rotating Bénard convection, Phys. Rev. Lett. 74, 530, (1995)) :

$$\begin{aligned}\dot{\psi}(\mathbf{x},t) = &\left[\epsilon - (k_c^2 + \Delta)^2\right]\psi(\mathbf{x},t) - \alpha\left[\alpha\psi(\mathbf{x},t)^2 + (\nabla\psi(\mathbf{x},t))^2\right] \\ &+ \nabla\cdot\{\nabla\psi(\mathbf{x},t)\left[\alpha\psi(\mathbf{x},t)^2 + (\nabla\psi(\mathbf{x},t))^2\right] \\ &- Ta\beta\nabla\{\times\mathbf{e}_z\times\nabla\psi(\mathbf{x},t)\left[\alpha\psi(\mathbf{x},t)^2 + (\nabla\psi(\mathbf{x},t))^2\right]\}\end{aligned} \tag{1.55}$$

For $Ta = 0$ we find the following Ljapunov functional

$$V[\psi] = \int d\mathbf{x} \left[-\frac{1}{2}\{\epsilon\psi^2 - \left[(k_c^2 + \Delta)\psi\right]^2\} + \frac{1}{4}\left[\alpha\psi^2 + (\nabla\psi)^2\right]^2 \right] \tag{1.56}$$

The evolution equation, therefore, has the general form

$$\dot{\psi} = -\frac{\delta}{\delta\psi}V - TaM[\psi] \tag{1.57}$$

By varying the Taylor number, it is possible to gradually turn on non-variational effects.

Amplitude Equation

The ansatz

$$\psi(\mathbf{x}, t) = \sum_{\mathbf{k}} A_{\mathbf{k}}(t) e^{i\mathbf{k}\cdot\mathbf{x}} \qquad , \qquad k = k_c = 1 \tag{1.58}$$

leads to the set of amplitude equations

$$\dot{A}_{\mathbf{k}} = \epsilon A_{\mathbf{k}} - S A_{\mathbf{k}} |A\mathbf{k}|^2 - A_{\mathbf{k}} \sum_{\mathbf{k}' \neq \mathbf{k}} (S + W_{\mathbf{k},\mathbf{k}'}) |A_{\mathbf{k}'}|^2 \tag{1.59}$$

The straightforward calculation of the coefficients S, $W_{\mathbf{k},\mathbf{k}'}$ for the model equation yields

$$\begin{aligned} S &= 3\alpha^2 + 2\alpha + 3 \\ W_{\mathbf{k},\mathbf{k}'} &= S - 2 + 2cos2\Phi + 2Tasin2\Phi \end{aligned} \tag{1.60}$$

Here, Φ denotes the angle between the wave vectors $\mathbf{k}$, $\mathbf{k}'$.

Stripe Patterns

Roll solutions possess the amplitude

$$|A_{\mathbf{k}}|^2 = \frac{\epsilon}{S} \tag{1.61}$$

We consider now perturbations $A_{\mathbf{k}'}$ whose linear evolution is given by

$$\dot{A}'_{\mathbf{k}} = -\frac{\epsilon}{S} W_{\mathbf{k}',\mathbf{k}} A_{\mathbf{k}} \tag{1.62}$$

As a criterion for instability of rolls we obtain

$$W_{\mathbf{k},\mathbf{k}'} < 0 \tag{1.63}$$

Square Patterns

We first consider the case $\alpha = 0$. This case leads to the selection of square patterns. We explicitly obtain, considering the nonrotating case $Ta = 0$:

$$S = 3 \qquad , \qquad W = 1 + 2cos2\Phi \tag{1.64}$$

This indicates that rolls are unstable with respect to perturbations forming an angle larger than

$$\Phi = -\frac{1}{2}arccos\frac{1}{2} \tag{1.65}$$

The most unstable modes are disturbances with $\Phi = 90$, which indicates the selection of *square patterns.*

Küppers-Lortz Instability

Roll solutions possess the amplitude

$$|A_{\mathbf{k}}|^2 = \frac{\epsilon}{S} \tag{1.66}$$

We consider now perturbations $A_{\mathbf{k}'}$ whose linear evolution is given by

$$\dot{A}'_{\mathbf{k}} = -\frac{\epsilon}{S}W_{\mathbf{k}',\mathbf{k}}A_{\mathbf{k}} \tag{1.67}$$

As a criterion for instability of rolls we obtain

$$W_{\mathbf{k},\mathbf{k}'} < 0 \tag{1.68}$$

This gives us the condition

$$2Tasin2\Phi \geq S(\alpha) - 2 + 2cos2\Phi \tag{1.69}$$

For each Taylor number, there is a critical angle, at which the instability sets in. This number is given by

$$Ta = \left[\frac{S}{2} - 1 + cos2\Phi\right] / sin2\Phi \tag{1.70}$$

The minimum Taylor number is obtained for a critical angle Φ_c, which is calculated to be determined by

$$\frac{\partial}{\partial\Phi}Ta(\Phi) = 0 \tag{1.71}$$

A straightforward calculation yields

$$cos2\Phi_c = -\frac{2}{S-2} \tag{1.72}$$

and the corresponding critical Taylor number is

$$Ta_c = \sqrt{(S/2-1)^2 - 1} = \sqrt{\frac{S^2}{4} - S} \tag{1.73}$$

We can now determine the value of α, which corresponds to the critical angle of 60. This yields

$$cos120 = -\frac{1}{2} = -\frac{2}{S-2} \tag{1.74}$$

This is achieved for the value

$$\alpha_{60} = \frac{1+\sqrt{10}}{3} \approx 1.38 \tag{1.75}$$

1.9.2 Model for Spiral Turbulence

A highly interesting pattern forming process can be detected in Rayleigh-Bénard convection in fluids which are characterized by a low Prandtl number, i.e. by a small ratio of kinematic viscosity and heat conductivity. These fluids are only slightly viscous but can well conduct heat. The low viscosity of the fluid has the consequence that vortical motions, i.e. nearly two dimensional fluid motions in the horizontal plane, are only slightly damped and can interfere with the dynamics of the convection rolls. This has the consequence that in addition to the order parameter field $\psi(\mathbf{x}, t)$ a vortical velocity field has to be taken into account.

We denote the vortical flow (quite often also denoted as mean flow) by $\mathbf{V}(\mathbf{x}, t)$. Since the mean flow is two dimensional it can be derived from a stream function $\chi(\mathbf{x}, t)$. As is well-known the stream function of a two dimensional flow obeys the evolution for the stream function

$$\dot{\Delta}\chi(\mathbf{x},t) + \frac{\partial}{\partial x}\Delta\chi\frac{\partial}{\partial y}\chi(\mathbf{x},t) - \frac{\partial}{\partial x}\chi\frac{\partial}{\partial y}\Delta\chi(\mathbf{x},t) = f(\mathbf{x},t) \tag{1.76}$$

External forcing is included in terms of $f(\mathbf{x}, t)$. The stream function is a secondary order parameter field, which is forced by convective motion.

A detailed analysis performed by Manneville et al. leads to a generalization of the Swift-Hohenberg equation including a *mean flow*

$$\begin{aligned}
&\dot{\psi}(\mathbf{x},t) + \mathbf{u}(\mathbf{x},t)\cdot\nabla\psi(\mathbf{x},t) = \left[\epsilon - (k_c^2 + \Delta)^2\right]\psi(\mathbf{x},t) + N\left[(\mathbf{x},t)\right] \\
&\mathbf{u}(\mathbf{x},t) = -\nabla\times\mathbf{e}_z\chi(\mathbf{x},t) \\
&\quad\dot{\Delta}\chi = \left[-\gamma + \Delta\right]\Delta\chi + \delta\mathbf{e}_z\cdot\left[\nabla\psi(\mathbf{x},t)\times\nabla\Delta\psi(\mathbf{x},t)\right]
\end{aligned} \tag{1.77}$$

The vortical motion is assumed to be weak so that nonlinearities in the equation for the stream function can be neglected. The coupling between the two fields is the transport of the convective rolls due to vortical motion on the one hand side and excitation of fluid motion by convection. (P. Manneville, J. Phys. 44, 759 (1983), P. Manneville, J. Phys. 44, L-903 (1983))

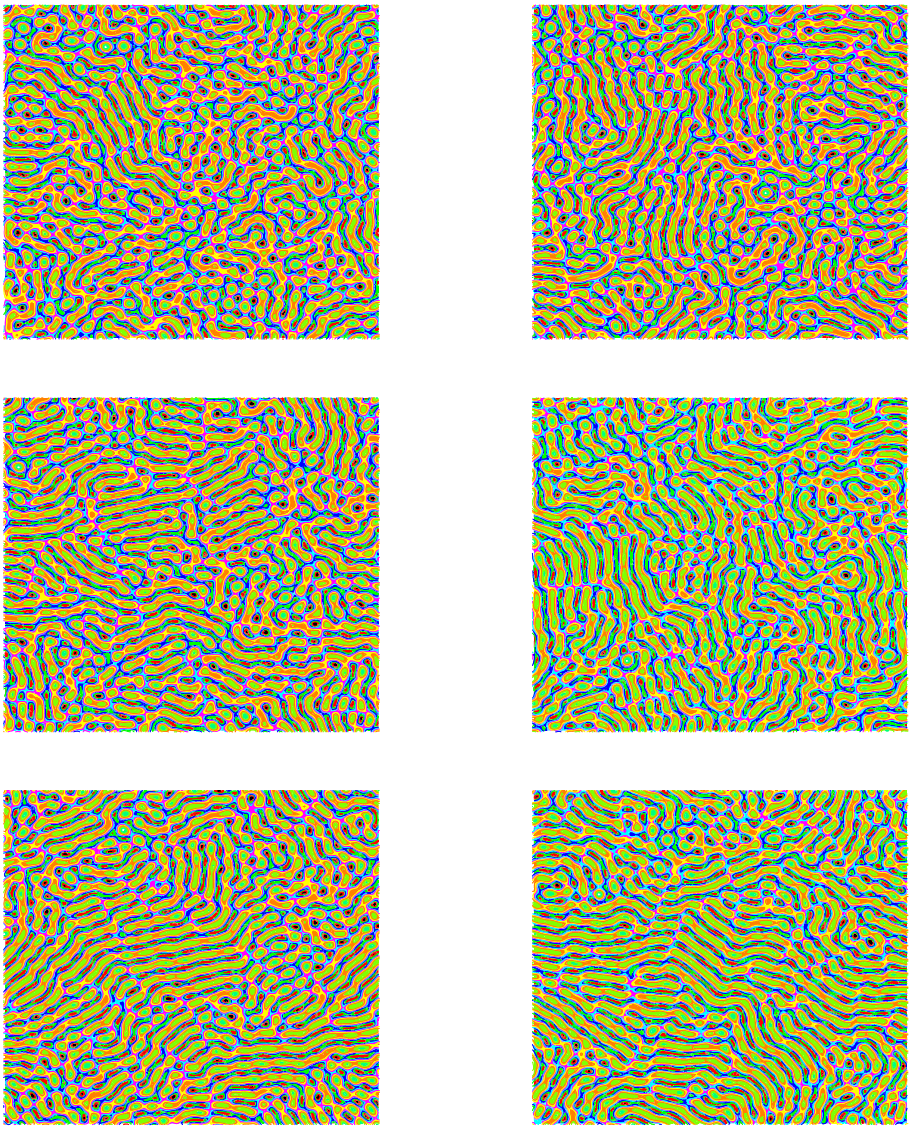

Fig. 1.12. Numerical Calculation of the evolution of patterns exhibiting a Küppers-Lortz type instability.

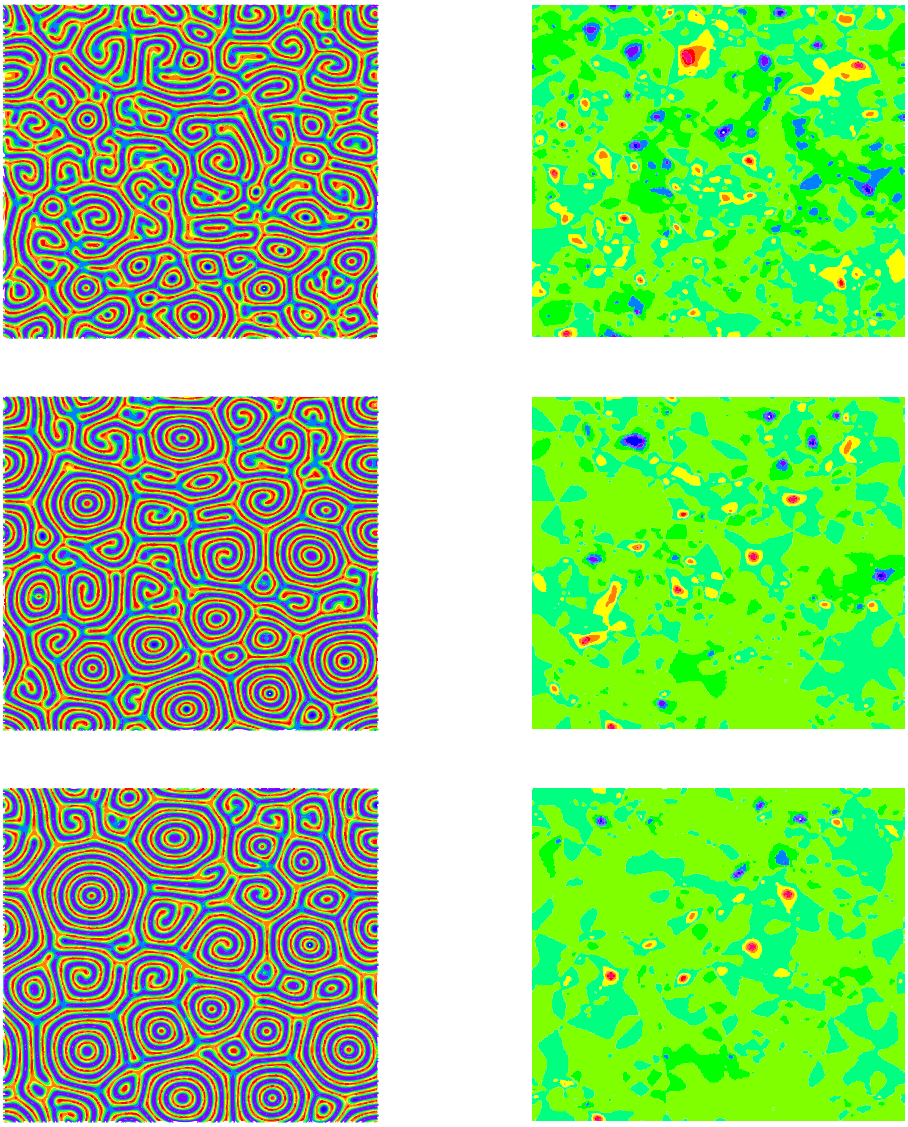

Fig. 1.13. Numerical Calculation of the evolution of patterns resembling spiral defect turbulence in Rayleigh- Bénard systems. The left side shows the order parameter field, which has to be identified with the temperature field. The right side exhibits the stream function χ related with the vortical motion in the plane.

Giant Spirals

We can generate giant spiral solutions using a circular domain and the boundary conditions

$$\psi_{\delta V} = d \qquad , \qquad \chi = 0 \tag{1.78}$$

For more information we refer the reader to M. Bestehorn, M. Fantz, R. Friedrich, H. Haken, C. Pérez-Garcia, Spiral patterns in thermal convection, Z. Phys. B 88, 93 (1992)).

Spiral Defect Turbulence

Figure (1.13) exhibits the spatio-temporal evolution of patterns generated by the model equation (1.77). for further details we refer to M. Bestehorn, M. Fantz, R. Friedrich, H. Haken, Hexagonal and spiral patterns of thermal convection, Phys. Lett. A 174, 48 (1993).

1.10 Complex Swift-Hohenberg Equations

It is well-known that nonequilibrium systems are capable of generating selfsustained temporal oscillations. A generic mechanism for the emergence of such oscillations is the so-called Hopf-bifurcation. A simple extension can be based on the amplitude equation, where we now assume that the linear growth rate is complex

$$\dot{\xi}_{\mathbf{k}} = \left[\epsilon + i\omega_0 + ib(k_c^2 - \mathbf{k}^2) - (1+ia)(k_c^2 - \mathbf{k}^2)^2\right] \xi_{\mathbf{k}} \tag{1.79}$$

This linear relation indicates that the mode amplitudes grow with the growth rate $\epsilon - (k_c^2 - \mathbf{k}^2)^2$ in an oscillatory way, where the frequency is

$$\omega = \omega_0 + b(k_c^2 - \mathbf{k}^2) - a(k_c^2 - \mathbf{k}^2)^2 \tag{1.80}$$

The linear field takes the form

$$\psi(\mathbf{x},t) = \sum_{\mathbf{k}} \frac{e^{i(\mathbf{k}\cdot\mathbf{x}-\omega t)} e^{\lambda_r(k)t}}{\sqrt{V}} \xi_{\mathbf{k}} + \frac{e^{i(\mathbf{k}\cdot\mathbf{x}+\omega t)} e^{\lambda_r(k)t}}{\sqrt{V}} \xi_{\mathbf{k}} \tag{1.81}$$

It is a superposition of traveling waves traveling in $\mathbf{k}$ and $-\mathbf{k}$ direction. A superposition of right and left traveling waves may also lead to standing waves.

In addition to the mechanisms of saturation of the amplitudes and the selection of patterns the nonlinearity now controls the selection of traveling waves versus standing waves. The following complex order parameter equation has been used to investigate these questions in some details:

$$\begin{aligned} \dot{\psi}(\mathbf{x},t) = & \left[\epsilon + i\omega i\alpha \left(k_c^2 + \Delta\right) - (1+ia)\left(k_c^2 + \Delta\right)^2\right] \psi(\mathbf{x},t) \\ & - A|\psi(\mathbf{x},t)|^2 \psi(\mathbf{x},t) - B|\nabla\psi(\mathbf{x},t)|^2 \psi(\mathbf{x},t) \\ & - C\left(\nabla\psi(\mathbf{x},t)\right)^2 \psi(\mathbf{x},t)^* \end{aligned} \tag{1.82}$$

For details we refer to the following publications: M. Bestehorn, H. Haken, Traveling waves and pulses in a two-dimensional large aspect ratio system, Phys. Rev. A 42, 7195 (1990)
M. Bestehorn, R. Friedrich, H. Haken, The oscillatory instability of a spatially homogeneous state in large aspect ratio systems of fluid dynamics, Z. Phys. B 72, 265 (1988)
M. Bestehorn, R. Friedrich, H. Haken, Traveling waves in nonequilibrium systems, Physica D 37, 295 (1989)
M. Bestehorn, R. Friedrich, H. Haken, Two dimensional travelling wave patterns in nonequilibrium systems, Z. Phys. B 75, 265 (1989)
M. Bestehorn, R. Friedrich, H. Haken, Modulated traveling waves in nonequilibrium systems: blinking state, Z. Phys. b 77, 151 (1989)